

UC Irvine

UC Irvine Previously Published Works

Title

A reaction study of sulfur vapor with silver and silver-indium solid solution as a tarnishing test method

Permalink

<https://escholarship.org/uc/item/1gq3w8hj>

Journal

Journal of Materials Science: Materials in Electronics, 27(10)

ISSN

0957-4522

Authors

Huo, Yongjun
Fu, Shao-Wei
Chen, Yi-Ling
[et al.](#)

Publication Date


2016-10-01

DOI

10.1007/s10854-016-5124-y

Peer reviewed

A reaction study of sulfur vapor with silver and silver–indium solid solution as a tarnishing test method

Yongjun Huo¹  · Shao-Wei Fu¹ · Yi-Ling Chen¹ · Chin C. Lee¹

Received: 17 February 2016 / Accepted: 3 June 2016 / Published online: 10 June 2016
© Springer Science+Business Media New York 2016

Abstract It is well known that pure silver (Ag) or sterling silver can easily get tarnished under ordinary atmosphere by sulfur-containing gases. Over past several decades, the industries have tried to formulate and produce silver-based materials that do not get tarnished for various applications including electronics, optics, jewelry, and silverware. Recently, our group has grown silver and silver–indium solid solution ingots and studied their anti-tarnishing property. Since there are no standard tarnishing test methods for Ag-based alloys, we have designed and established an accelerated tarnishing experiment using sulfur vapor as the reacting agent. Sulfur vapor, rather than other sulfur-containing gases such as H₂S, is chosen because sulfur vapor reacts with silver more easily to form silver sulfide (Ag₂S). After ingot growth, disk samples were cut from silver and silver–indium solid solution ingots and examined with X-ray diffraction (XRD) and scanning electron microscope/energy dispersive X-ray spectroscopy (SEM/EDX). Commercially available Argentium silver was also studied for comparison. Disk samples were placed into the sulfur vapor reacting chamber at 120 °C for 15, 30, 45, and 60 min, respectively. The thickness of Ag₂S film grown on the samples was measured. The results showed that Ag₂S growth rate depends on indium concentration. For example, with 19 at.% In, Ag₂S growth rate on silver–indium solid solution is only 4 % of that on pure silver and 7 % of that on Argentium silver. The excellent anti-tarnishing property of silver–indium solid solution should open up new

applications in electronics, jewelry, joining, optics, silverware, and welding.

1 Introduction

Silver possesses the title of champion for its highest thermal conductivity, electrical conductivity, and reflectivity among any known metal elements. Dry silver does not form a significant surface oxide at ambient temperature and pressure [1], so it is relatively chemical inert to oxidation under normal atmosphere. However, silver is very sensitive to the presence of sulfur-containing corrosive gases such as sulfur vapor, hydrogen sulfide, sulfur dioxide, and carbonyl sulfide, etc. Typically, the concentrations of those corrosive gases are very low, ranging from less than one parts per billion (ppb) under normal atmosphere to hundreds of ppb in heavy industrial environment [2]. However, the corrosion phenomenon can be commonly observed from silver used in electronics. The corrosive reaction product is silver sulfide which can be the killer of electronic products in several aspects. First of all, silver sulfide has poor mechanical strength, so it can be detached and crumbled from its substrate easily. In addition, the resistivity of silver sulfide is 7–10 order of magnitude higher than that of silver [3], so the overall resistivity will continue to increase with the formation of silver sulfide. Silver sulfide also poses a threat to circuits because its dendritic growth nature might result in the formation of silver sulfide whiskers [4]. This could lead to the occurrence of short circuit since silver sulfide is not a good insulating material either. Furthermore, the reflectance of silver mirror surface used in LEDs would drop significantly with corrosive degradation, resulting in light output power reduction [5].

✉ Yongjun Huo
yongjunh@uci.edu

¹ Electrical Engineering and Computer Science, Materials and Manufacturing Technology, University of California, Irvine, CA 92697-2660, USA

In order to understand the nature of silver sulfurization, extensive research has been conducted over the decades. Several experiments, using various corrosive gases, such as sulfur vapor [6], hydrogen sulfide [7], sulfur dioxide [8], and organic sulfur [9], have been performed to see the influence on the rate of silver tarnishing. Other environmental parameters, such as temperature, relative humidity [10], illumination [8], and silver surface state [11], have also been studied to explore the silver tarnishing mechanism, thereby searching possible scientific and engineering solutions for anti-tarnishing purposes. In literatures, some surface treatments for silver using different coating methods or coating materials such as metallic coating by electroplating [12], sputter-applied coatings [13], oxide coating [14], organic coating [15], chromate conversion coating [16], etc. However, such thin layer of coating material can be worn off very easily after a short period of time. Another approach to improve the anti-tarnishing property of silver is by alloying. Alloying with copper can strengthen silver, but it will make silver less tarnish resistant to corrosive gases [17]. It has been reported that adding other elements such as palladium [18], silicon [19], tin [20], germanium [21], and zinc [22], would have, more or less, increased anti-tarnishing effects compared with sterling silver. However, to the knowledge of the authors, there is no standard test method existing to quantify the capability of anti-tarnishing for different silver alloy.

Recently, the authors had presented some preliminary anti-tarnishing results of the silver solid solution phase with indium [23]. In the present work, we have designed a new quantitative test method and performed the reaction experiments with well-controlled and repeatable environments. The authors hope to establish this method as a standard anti-tarnishing test method for silver-based alloys. In the following sections, silver solid solution phase with indium, designated as (Ag)–xxIn in this paper, are produced in polycrystalline ingot form at two different compositions. After examining their chemical composition using SEM/EDX and XRD, the prepared samples are tested in the designed sulfurization experiment. The details of the design of the sulfurization test experiment have been described. Experimental results are reported, analyzed, and discussed. Finally, a summary is then given.

2 Material preparation and characterization

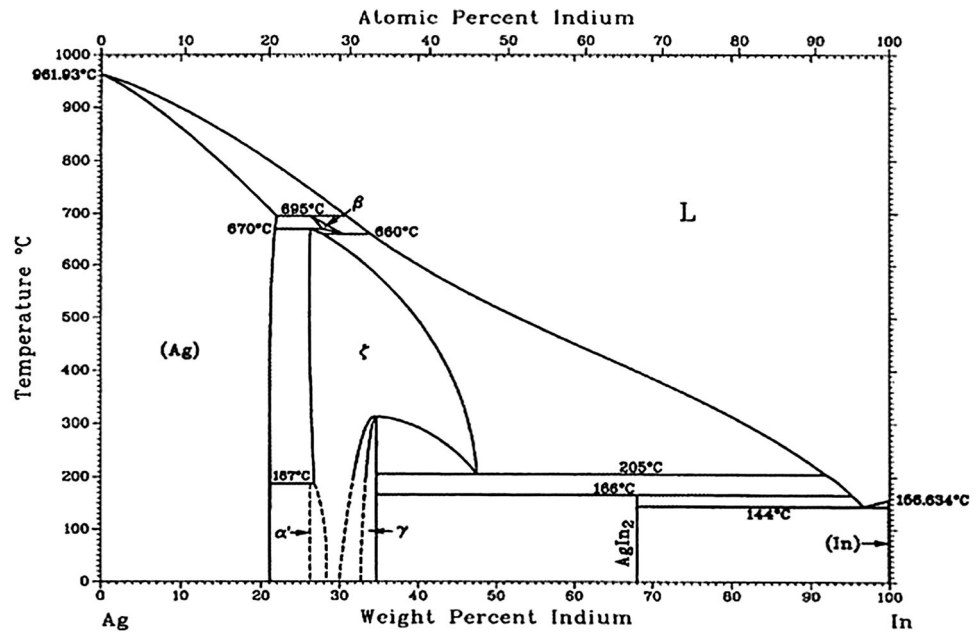
In order to understand Ag–In binary system and produce the single phase (Ag)–xxIn material, it is essential to review the Ag–In binary phase diagram, as shown Fig. 1 [24]. The maximum solubility of indium element in silver crystal lattice is 20 at.% at room temperature, the silver–indium solid phase with face-centered cubic (FCC) crystal

structure is designated as α phase historically. In the literature [25], the authors discovered α' phase, which has also cubic crystal structure, at the composition of 25 at.%, and it is correspond to Ag_3In which is transformed from ζ phase at 187 °C. It is important to note that material composition may fluctuate from region to region, which can be caused by various mechanism of segregation effects. Therefore, it is necessary to keep enough margin to the maximum solubility boundary in order to avoid entering the mixture region of α and α' phase in the phase diagram, thereby producing nearly homogeneous single phase silver–indium solid solution. As a consequence, (Ag)–xxIn with 19 at.% indium concentration has been chosen as the primary research subject, which is designated as (Ag)–19In in this article. In addition, (Ag)–9.5In with 9.5 at.% indium has been also produced and investigated in order to find influence of the indium concentration on the properties of (Ag)–xxIn phase.

The casting method was chosen for the production of the material of the interested phase, resulting in the form of ingots. The raw materials of silver and indium shots with 99.99 % purity were weighed, uniformly mixed and loaded in quartz tube with one end closed. Since the native oxide forming on the surface of silver and indium metal is negligible thin, there is no treatment required to perform before loading the raw material. While the quartz tube is being pumped by a vacuum pump, the other end of the tube is sealed by hydrogen–oxygen torch operation to form a capsule. The vacuum environment is necessary for the casting production for reducing the number of voids or common defects created by trapped air bubbles. Next, the capsule was placed into a furnace preheated at 1030 °C and stayed there for 30 min. The temperature of the furnace was then reduced gradually to room temperature in 7 days in order to obtain the homogenized single phase solid solution at different compositions. This is the preliminary process and optimization requires more time and many growth runs.

After the successful production of (Ag)–xxIn solid solution, the ingots were cut into disk samples, using slow speed diamond saw, for further chemical composition examination. X-ray diffraction (XRD) and scanning electron microscope/energy dispersive X-ray spectroscopy (SEM/EDX) were used in a combination to identify (Ag)–xxIn phase, since their functionality are complementary to each other. While SEM/EDX can provide information about specific chemical composition at local areas within its electron-beam interaction volume, a few micron meters or sub-micron range depending on the electron beam energy and atomic number of the material under examination. On the other hand, XRD is capable of interpreting the crystallography nature of the material by generalizing data generated from macroscopic regions of the samples,

Fig. 1 Silver–indium binary phase diagram



thereby identifying the phases of the unknown material precisely and accurately. Before material characterization, the disk samples were prepared by polishing process in the sequence of 120/240/800/1200 grits, using silicon carbide abrasive papers.

FEI/Philips XL-30 FEG SEM in the Laboratory for Electron and X-ray Instrumentation (LEXI) was used for the SEM/EDX examination. Several local areas of the disk samples were randomly chosen to be examined by SEM/EDX. For example, as shown in Fig. 2, nine points of interests have been examined by SEM/EDX at 1000 \times magnification for each (Ag)–9.5In and (Ag)–19In disk samples respectively, and the results of chemical compositions are listed in Table 1.

According to the SEM/EDX machine setting, the error of compositions are ± 0.88 and ± 0.54 at.% for Ag and In respectively. Therefore, the variation of chemical compositions for the data shown in Table 1 is within the range of the error that due to the uncertainty of the SEM/EDX detector, except for a few points deviation from the intended value.

After determination of the chemical composition, Rigaku SmartLab X-ray diffractometer in LEXI was used for further phase identification, using Bragg–Brentano (BB) operation mode with θ – θ diffractometer setting. During XRD examination, the disk sample remains stationary and the detector and X-ray source rotate at the same angular speed. To be more specific, the XRD measurement conditions and parameters are summarized in Table 2. The results of XRD examination for (Ag)–9.5In and (Ag)–19In disk samples are shown in Fig. 3, with pure Ag disk sample XRD result as reference. The XRD measurement data have

been collected and analyzed by PDXL, an integrated powder X-ray analysis software package. The crystallography information for the silver–indium solid solution can be learned thusly from the XRD diffraction, which is listed in Table 3.

As shown Fig. 3, it is very clear that (Ag)–9.5In and (Ag)–19In resemble the crystal structure of pure silver, face-centered cubic (FCC) crystal structure, for its typical systematically peaks absence. In addition, there are no major peaks other the peaks of Ag, (Ag)–9.5In, (Ag)–19In in each XRD patterns. Therefore, it can be safely concluded that the materials in the disk samples are nearly homogeneous and polycrystalline. In Table 3, (h, k, l) is the Miller's indices with classic denotation, d is the d-spacing value for corresponding crystal plane, and a is the calculated lattice constant by using the values of each d-spacing. As results, the X-ray diffraction patterns have shifted towards left as the indium concentration increases, which is corresponding to the increasing values of lattice constants from pure Ag, (Ag)–9.5In to (Ag)–19In. The weighted average values for lattice constants are 4.092, 4.126, and 4.153 Å for pure Ag, (Ag)–9.5In, and (Ag)–19In respectively. The trend of increasing values for lattice constants can be explained by reviewing atomic radius for silver and indium elements. The atomic radius for indium, 167 pm, is larger than that of silver atom, 144 pm, so that if one substitutes silver atoms with indium atoms in the original FCC lattice sites, it would result in the bulge in its crystal structure, thereby increasing the values of the lattice constants as indium concentration increased. In other words, one could reversely determine the indium concentration in (Ag)–xxIn solid solution by examine the lattice

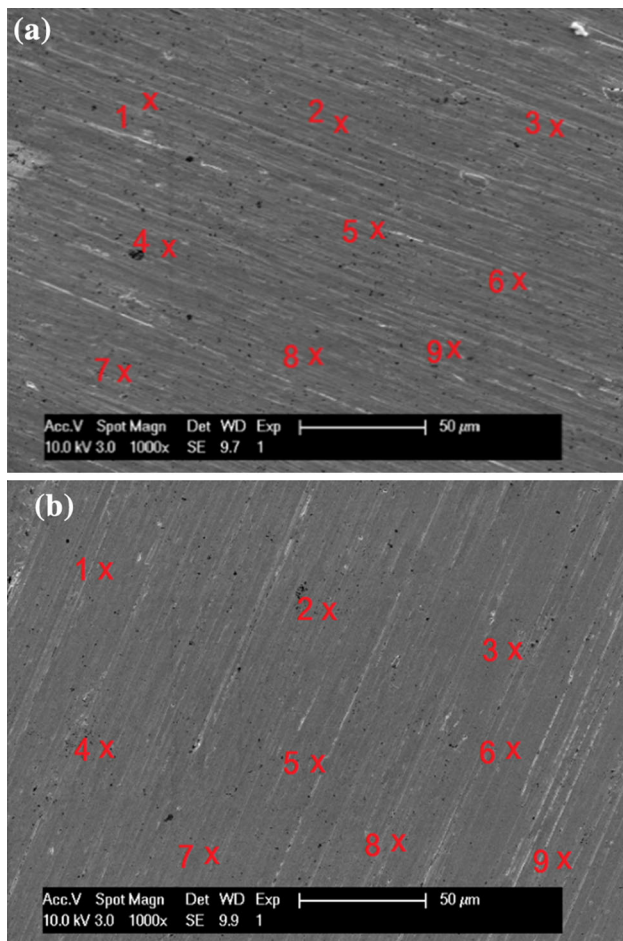


Fig. 2 **a** (Ag)–9.5In disk SEM/EDX tested region, **b** (Ag)–19In disk SEM/EDX tested region

Table 1 SEM/EDX results of chemical compositions for (Ag)–9.5In and (Ag)–19In disk in the tested region

	(Ag)–9.5In		(Ag)–19In	
	Ag (at.%)	In (at.%)	Ag (at.%)	In (at.%)
1	90.97	9.03	81.73	18.27
2	90.92	9.08	81.43	18.57
3	91.32	8.68	81.24	18.76
4	91.23	8.77	80.61	19.39
5	92.28	7.72	82.24	17.76
6	90.01	9.99	81.54	18.46
7	90.60	9.40	81.01	18.99
8	90.91	9.09	81.39	18.61
9	90.72	9.28	80.68	19.32

constant value using XRD for unknown compositions in the future study. Even though the authors have the awareness of that the radius for silver and indium metallic ions in the metal are different from the values of their

atomic radius of solo atoms, the general principle must be plausible for this analysis approach.

The SEM/EDX and XRD results shown above are representatives for disk samples’ chemical composition and crystallography examination, and results in general are similar and repeatable for different examined regions, disk samples, and ingots. In conclusion, our research group has been successfully grown the nearly homogeneous and polycrystalline (Ag)–9.5In and (Ag)–19In ingots, using the casting method in a quartz capsule with vacuum pumped and specific annealing profiles within the laboratory and research facility. However, there are still some space for improvement in terms of the ingots growth procedure and annealing profile design.

Argentium silver is one of commercially available sterling silver with claimed good anti-tarnishing property [21]. Germanium is used as alloying element to protect the silver by forming a thin layer of germanium oxide on the surface of this silver alloy. Argentium silver was purchased from local vendor in sheet form, and then cut into disk samples. The compositions of the Argentium silver are 93.5 at.% of Ag, 5 at.% of Cu, and 1.5 at.% of Ge in average, according to the vendor material data sheet and our EDX data. In addition, pure silver has also been grown using the same casting method. In this research, pure silver and Argentium silver were used as reference controlled group to compare with (Ag)–xxIn solid solution in the following experiments.

3 Design of sulfurization experiment

In measuring anti-tarnishing property of silver and its alloys, we have not been able to find a standard test method or a repeatable test method in literature. We have thusly designed a set of experiments to quantitatively study the chemical reaction between sulfur-containing corrosive gas and (Ag)–xxIn solid solution and other silver-based alloys. Since sulfur is the element essentially responsive to the corrosive behavior of silver tarnishing, sulfur vapor (S_n) and hydrogen sulfide gas (H₂S) would be plausible corrosive gas candidates for this experiment. In literature [26], the reaction between silver and hydrogen sulfide as shown in Eq. (1) is endothermic, where the change of enthalpy is ΔH = +10 kJ/mol. In ambient environment, the hydrogen sulfide can corrode silver as in Eq. (2). However, it cannot react with silver without heating or oxidizing agent.

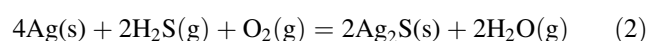
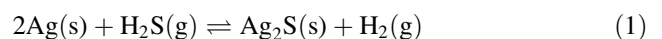


Table 2 A summary of Rigaku SmartLab X-ray diffractometer measurement conditions and parameters

X-ray source	40 kV, 44 mA	Scan speed/duration time	2.0000°/min.
Goniometer	None	Step width	0.0200°
Attachment	None	Scan axis	2Theta/Theta
Filter	Cu_K-beta	Scan range	20.0000°–90.0000°
CBO selection slit	None	Incident slit	2/3°
Diffracted beam mono.	None	Length limiting slit	None
Detector	D/teX ultra	Receiving slit #1	4.000°
Scan mode	Continuous	Receiving slit #2	13.000 mm

On the other hand, the reaction between silver and sulfur vapor shown in Eq. (3) is exothermic, where the change of enthalpy is $\Delta H = -32$ kJ/mol. The sulfur vapor can corrode silver without heating or other gases involved. It is much easier to control on the concentration of one species of vapor than two species in the experiment system. In addition, the reaction between the sulfur vapor and silver is thermodynamically preferable, so corrosion environment of sulfur vapor is more severe than that of hydrogen sulfide gas. Accordingly, the authors selected the sulfur vapor as the corrosive gas for the design of this accelerated quantitative corrosion test experiment.

In the following steps, pure silver, Argentium silver, (Ag)–9.5In and (Ag)–19In disk samples were prepared by polishing using 800 and 1200 grits abrasive paper. Finally, the disk samples preparation finished with mirror surface using 0.5 micron diamond suspension polishing process.

In order to evaluate the rate of chemical reaction between sulfur and silver quantitatively, the amount of resultant, i.e., silver sulfide, need to be measured. Therefore, the authors designed a technique to measure the thickness of silver sulfide layer by creating a sharp step (boundary) between reacted region and untouched region on the samples. First of all, all of the samples were evaluated in terms of surface roughness using the Dektak XT profilometer in Integrated Nanosystems Research Facility (INRF). The Dektak XT is a profilometer that provides quantitative data about sample's surface by using a contact measurement technique. Measurements are made by a diamond tipped stylus moving laterally in contact with a sample across a specified distance with a specified force with a resolution of 0.5 nm across a variety of surfaces. Typical root-mean-square (RMS) values of surface roughness are on the order of 50 nm. Next, the authors coated a layer of photoresist, AZ 4620, on half of the sample surface, followed by baking the samples at 120 °C for 10 min and baking the samples at 140 °C for 5 min. The resulting photoresist layer blocks the sulfur vapor from reaching the sample surface. An experiment was conducted to confirm that it was indeed the case.

As shown in Fig. 4, a closed system was designed to conduct the sulfurization experiment. The reaction chamber is a glass jar of 1 L volume having lid sealed with

rubber which can also be tightened up, thereby ensuring no leakage of sulfur vapor to the outside environment during experiment. Precipitated sulfur S595-500 was used as the sulfur vapor source. The melting temperature of sulfur 115.21 °C, so 120 °C is enough to completely melt the sulfur into liquid phase, thereby generating sulfur vapor through thermal evaporation. As shown in Fig. 5 [27], most of sulfur vapor molecules would be in the form of S_8 , so the total sulfur vapor pressure at thermal equilibrium is almost equal to partial vapor pressure of S_8 . After calculation using ideal gas law, if supplied with 5 mg sulfur element in weight, it would be enough for the sulfur vapor to reach the saturation point of vapor pressure at 120 °C. Considered the sulfur gas could be consumed continually during the reactions, the authors decided to oversupply the amount of precipitated sulfur in order to ensure that sulfur vapor concentration remains as a constant during the sulfurization experiment. As a result, 100 mg of precipitated sulfur was placed inside a small beaker which sit at the center of the reaction chamber during reaction. For one around of sulfurization experiment, disk samples of pure silver, argentium silver, (Ag)–9.5In and (Ag)–19In were put inside of the reaction chamber and evenly distributed near the sulfur containing beaker. After sulfurization experiment, the photoresist was removed by soaking into AZ 400T stripper at 70 °C for 2 min, leaving silver sulfide layer untouched. A separate experiment was conducted to confirm that the stripper did not attack the silver sulfide layer. After removing the photoresist, a step of silver sulfide layer was formed between the untouched and reacted regions. Finally, the step height was measured using Dektak XT profilometer. For example, the result has been illustrated for the profilometer measurement of the step height of silver sulfide layer on pure silver disk sample after 60 min sulfurization experiment. As shown in Fig. 6, the total length of profilometer scanning is 300 μm , and the sharp step of the silver sulfide layer is placed near the center of the scanning profile. The silver sulfide layer is not as smooth as the mirror finished silver surface due to the nature of silver sulfide film growth. Therefore, it is necessary to use statistical approach to evaluate the average film thickness. As a result, using the controlling software of Dektak XT profilometer, the RMS height values of selected

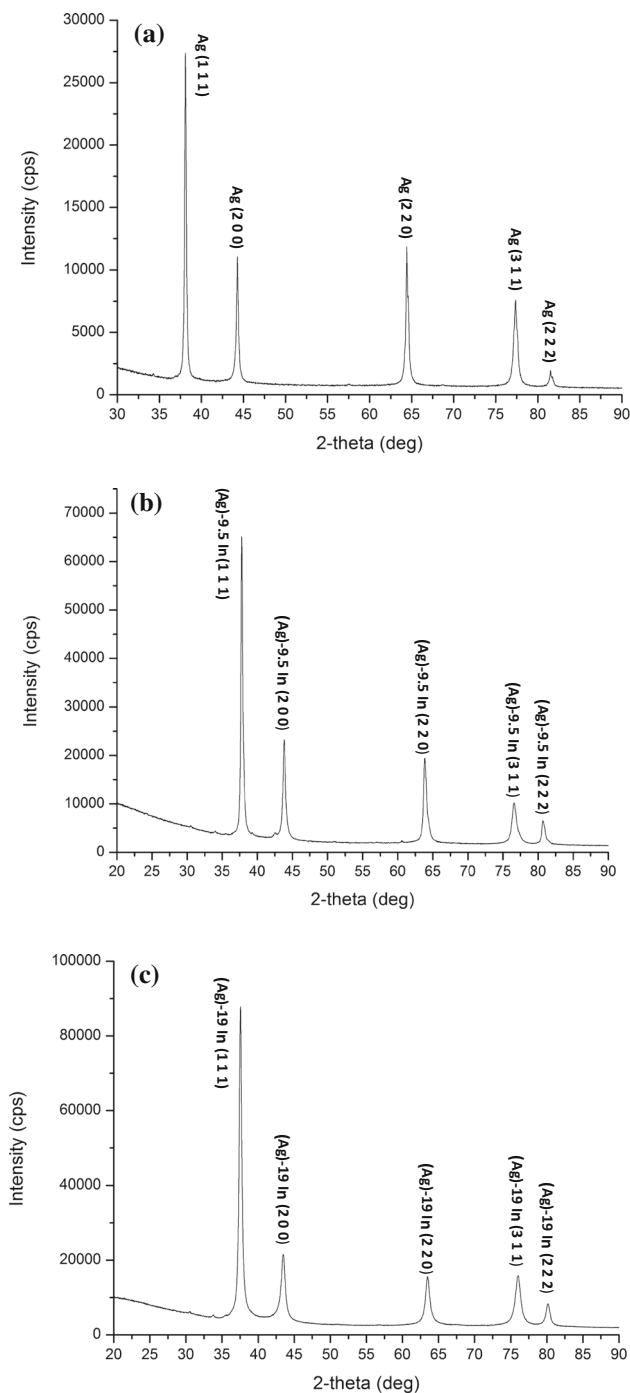


Fig. 3 a XRD pattern of pure silver disk sample, b XRD pattern of (Ag)-9.5In disk sample, c XRD pattern of (Ag)-19In disk sample

red region (reacted region) and green region (protected region) can be evaluated upon the measurement, where the typical length of selected area is from 50 to 60 μm. Thus, the difference between RMS values of reacted region and protected region can be determined, and then recorded as the step height value of the profilometer measurement.

Table 3 (a) A summary of XRD measurement data of pure silver disk sample after PDXL analysis, (b) a summary of XRD measurement data of (Ag)-9.5In disk sample after PDXL analysis, (c) a summary of XRD measurement data of (Ag)-19In disk sample after PDXL analysis

Peaks #	2θ (°)	d (Å)	(h, k, l)	a (Å)
(a)				
1	38.089	2.363	(1 1 1)	4.092
2	44.265	2.046	(2 0 0)	4.092
3	64.412	1.447	(2 2 0)	4.092
4	77.362	1.234	(3 1 1)	4.093
5	81.510	1.181	(2 2 2)	4.091
(b)				
1	37.769	2.380	(1 1 1)	4.122
2	43.825	2.067	(2 0 0)	4.134
3	63.816	1.457	(2 2 0)	4.121
4	76.572	1.244	(3 1 1)	4.126
5	80.679	1.191	(2 2 2)	4.126
(c)				
1	37.531	2.394	(1 1 1)	4.147
2	43.474	2.082	(2 0 0)	4.164
3	63.423	1.467	(2 2 0)	4.149
4	75.947	1.253	(3 1 1)	4.156
5	80.179	1.197	(2 2 2)	4.147

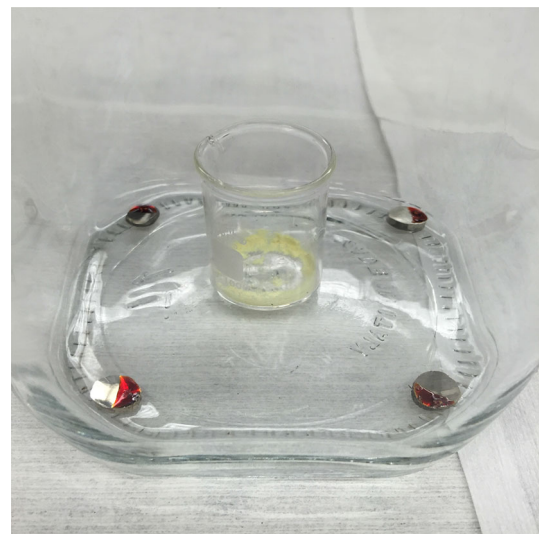


Fig. 4 The configuration of the designed closed system for sulfurization experiment

4 Experimental results and discussions

The purpose of the sulfurization experiment in this research is to evaluate the anti-tarnishing property of (Ag)-9.5In and (Ag)-19In, compared with pure silver and Argentium silver quantitatively. The authors studied the growth rate of

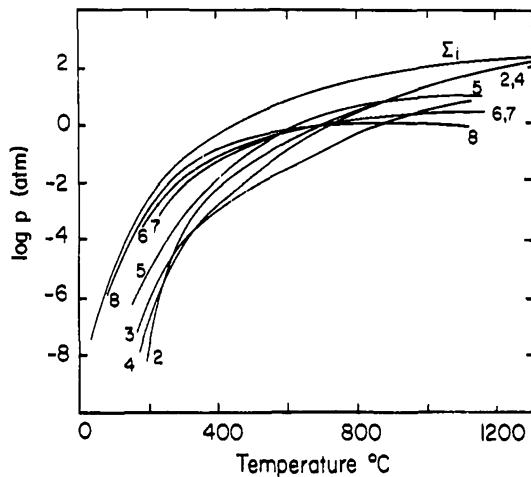


Fig. 5 Equilibrium pressure of sulfur, Σ_i is the total pressure, $2 \leq n \leq 8$, is the partial pressures of S_n

silver sulfide layer, i.e., the thickness of silver sulfide layer varying with time. Based on the assumption that the material medium is continuous and the law of mass conservation, the authors can calculate that the thickness of silver sulfide layer is 2.5 times of the value of measured step height that obtained from profilometer measurement, considering the silver sulfide layer growth is bidirectional at the initial solid–gas interface. The time length of the sulfurization experiments have set as 15, 30, 45, and 60 min respectively. After the experiments, the top-view images of the steps between the protected region and reacted region were taken, using the digital optical microscope. The images were taken at $500\times$ magnification using $50\times$ objective lens. At this magnification, the depth of focus of the objective is in the range of $\pm 0.3 \mu\text{m}$. As shown in Fig. 7, the surface of pure silver, Argentium silver, (Ag)–9.5In, and (Ag)–19In samples were observed under optical microscope after 15 min sulfurization

experiment. It is clear that the color of right hand side of the samples are still silvery, which means the applied photoresist protect the samples surface very well, so that the protected area of the samples remain inert to sulfur gas during the sulfurization. Furthermore, the author can observe left hand side of pure silver sample surface has been already blackened by the sulfur gas, even if the experiment time is only 15 min, as a result of the severity of corrosion environment of the designed experiment. The grains of silver sulfide can be clearly observed on the surface of pure silver sample, shown in Fig. 7a. As shown in Fig. 7b, Argentium silver reacted with sulfur vapor, resulting in forming the silver sulfide in islands form. The average size of islands of silver sulfide is about $5 \mu\text{m}$, and RMS value of the thickness of the islands is $0.45 \mu\text{m}$. Therefore, Argentium silver exhibits anti-tarnishing property to some extent if compared with pure silver, since it didn't form the continuous silver sulfide layer as pure silver did. In contrast, as shown in Fig. 7c, the color of the surface of (Ag)–9.5In sample is gray, meaning the formation of silver sulfide layer is much thinner than pure silver. Remarkably, as shown in Fig. 7d, the appearance of the (Ag)–19In sample is still silvery, even though a little bit of yellowish color in combine. As shown in Fig. 8, the pure silver and (Ag)–9.5In samples have been corroded further by the sulfur gas, as the experimental time increases to 30 min, since the color of reacted regions is darker than the previous ones. The authors can observe that a continuous film of silver sulfide start to form on the surface of (Ag)–9.5In sample. As shown in Fig. 8b, the Argentium silver sample surface preserved the island-like morphology after reacting with sulfur vapor for 30 min, and the average size of silver sulfide islands increases to $10 \mu\text{m}$, and RMS value of the thickness of the islands has increased to $1.30 \mu\text{m}$. In contrast, as shown in Fig. 8d, the reacted region of (Ag)–19In still remains yellowish, but darkened a little bit

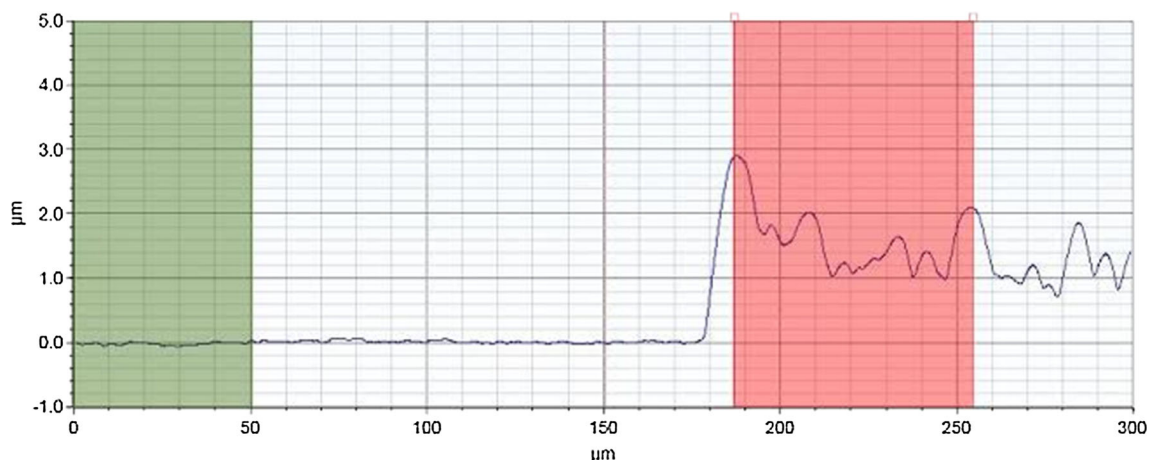


Fig. 6 Dektak XT Profilometer measurement profile of silver sulfide layer on pure silver sample

Fig. 7 **a** The top-view optical microscope image of pure silver disk sample, **b** of Argentium silver disk sample, **c** of (Ag)–9.5In disk sample, **d** of (Ag)–19In disk sample after 15 min sulfurization experiment

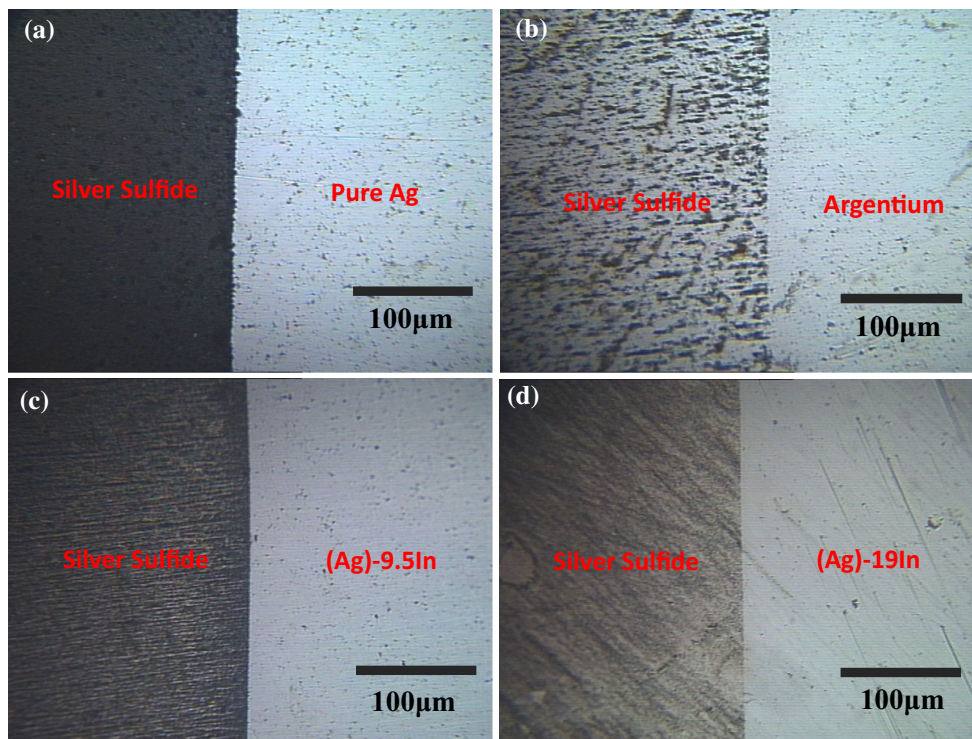
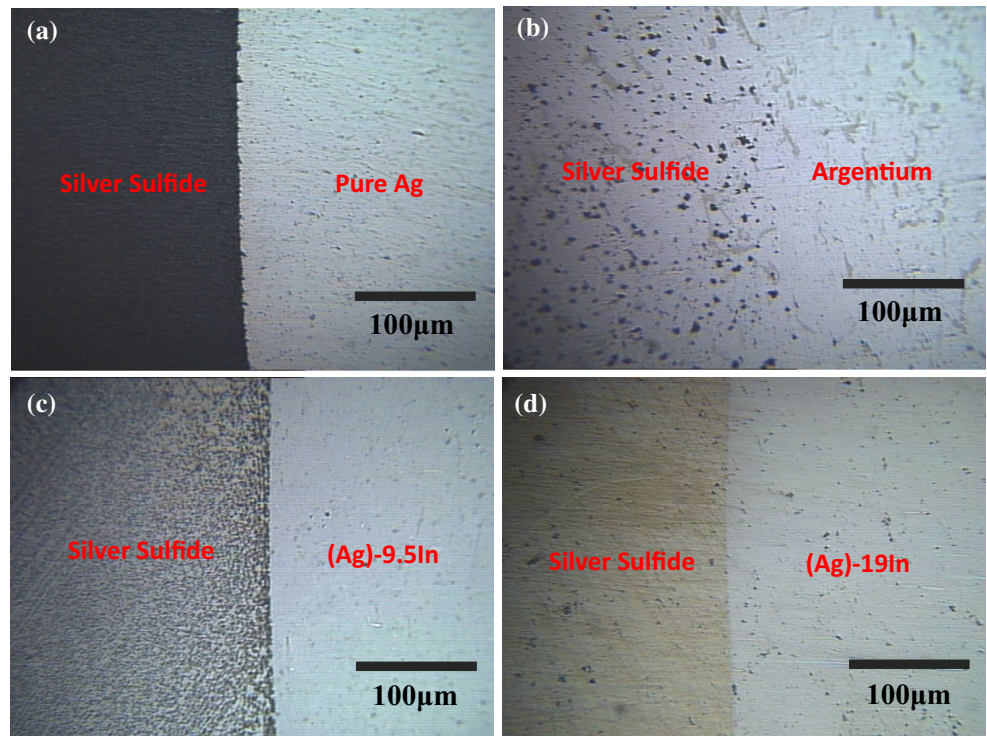


Fig. 8 **a** The top-view optical microscope image of pure silver disk sample, **b** of Argentium silver disk sample, **c** of (Ag)–9.5In disk sample, **d** of (Ag)–19In disk sample after 30 min sulfurization experiment

compared with the one in the 15 min experiment. When the experimental time increases to 60 min, the trend of corrosion for pure silver and (Ag)–9.5In samples continues, as

opposed to the (Ag)–19In samples remains relatively inert to sulfur gas corrosion, as shown in Fig. 9. As shown in Fig. 9b, the island-like morphology on the argentium silver

sample surface has changed, which means the islands of silver sulfide have been grown and coalesce with each other, resulting in forming the continuous film of silver sulfide. Therefore, through the direct observation of optical microscope image, the authors can conclude that silver indium solid solution exhibits a great anti-tarnishing property, and the ability of anti-tarnishing increases with the indium element concentration. As compared with Argentium silver, the (Ag)–19In exhibits better anti-tarnishing property.

After measuring by Dektak XT profilometer, the RMS values of the step height were recorded, so that the corrosion film thickness, i.e., the thickness of silver sulfide layer, can be calculated. The experimental data of the sulfurization test are collected and summarized in Table 4. In the literature [28], the reaction between silver and sulfur-based corrosion gas has a linearly time dependent relationship. Our experimental data of pure silver, (Ag)–9.5In and (Ag)–19In agrees with this linear relationship, and can be fit well into linear curves, as shown in Fig. 10. The slope of the linear curves are the corrosion rates in the environment of the designed sulfurization experiment for pure silver, (Ag)–9.5In and (Ag)–19In. After calculation, the corrosion rate of pure silver is $1.14 \times 10^{-3} \mu\text{m/s}$. The corrosion phenomenon in Argentium deviate from this linear assumption. The data

of argentium silver can be fit into two piecewise-linear curve. The initial corrosion rate is $7.25 \times 10^{-4} \mu\text{m/s}$ when the samples exhibit island-like morphology. After the coalescence of the islands, the corrosion rate accelerated to $1.50 \times 10^{-3} \mu\text{m/s}$, which is even higher than pure silver. Silver and copper can hardly be dissolved into each other crystal lattice at room temperature [29]. Therefore, the Argentium silver is essentially two phase alloy, which has Ag-rich phase and Cu-Ge rich phase [30]. It would explain why the argentium silver samples exhibit island-like morphology for short-term sulfurization reaction. Upon the coalescence of the islands, the silver sulfide layer become continuous, then continuous film morphology will be exhibited. On the other hand, our grown (Ag)–xxIn solid solutions have only single phase, so they would follow the linear growth behavior during sulfurization experiment. The corrosion rate of (Ag)–9.5In is $3.3 \times 10^{-4} \mu\text{m/s}$, which is 3.4 times slower than that of pure silver and 2.2 times slower than that of initial stage of argentium. Significantly, the corrosion rate of (Ag)–19In disk samples is only $5 \times 10^{-5} \mu\text{m/s}$, which is 22.8 times slower than of pure silver, 14.5 times slower than of initial stage of Argentium silver and 6.6 times slower that of (Ag)–9.5 In.

Using the corrosion rates obtained above, an exponential Eq. (4) can be extrapolated from the experimental data to

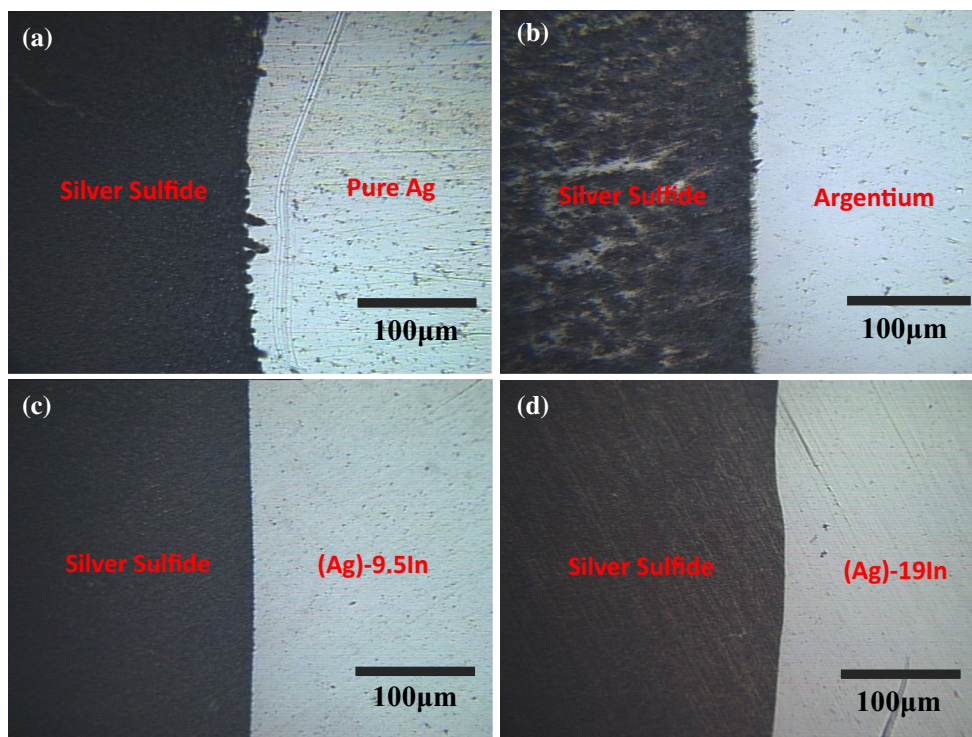


Fig. 9 **a** The top-view optical microscope image of pure silver disk sample, **b** of Argentium silver disk sample, **c** of (Ag)–9.5In disk sample, **d** of (Ag)–19In disk sample after 60 min sulfurization experiment

Table 4 A summary of sulfurization experimental results of Argentium silver, (Ag)–9.5In and (Ag)–19In with pure silver in comparison

Time (min)	Pure Ag	Argentium	(Ag)–9.5In	(Ag)–19In
Measured step height (μm)				
15	0.34	0.18	0.15	0.04
30	0.72	0.52	0.27	0.05
45	1.20	1.09	0.39	0.07
60	1.61	1.60	0.48	0.08
Film thickness (μm)				
15	0.85	0.45	0.38	0.10
30	1.80	1.30	0.68	0.13
45	3.01	2.73	0.98	0.18
60	4.03	4.01	1.20	0.20
Corrosion rate (μm/s)				
	1.14×10^{-3}	7.25×10^{-4}	3.33×10^{-4}	5.00×10^{-5}
		1.50×10^{-3}		

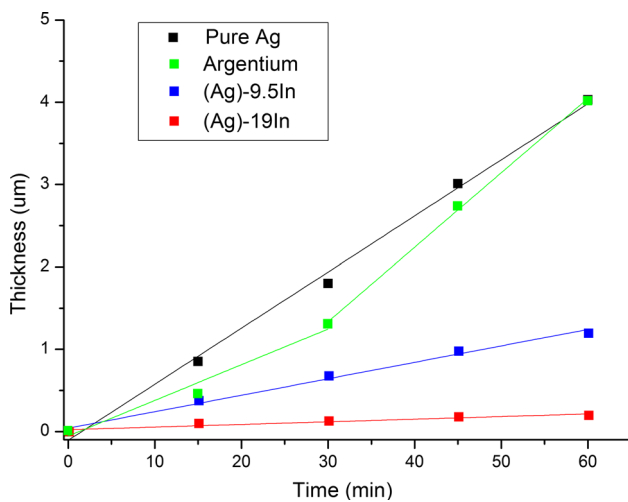


Fig. 10 The plot of silver sulfide layer thickness versus time after sulfurization experiments for pure silver, Argentium silver, (Ag)–9.5In, and (Ag)–19In disk samples

describe the correlation of growth rate of silver sulfide film and indium concentration of (Ag)–xxIn solid solution,

$$K = A * \exp(-x/t) + b \tag{4}$$

where the K is the corrosion reaction rate (Å/s), x is the indium concentration (at.%) of (Ag)–xxIn solid solution, A is the pre-exponential factor, which has the value of 12.55 Å/s, and t and b are both fitting constants, which have the numerical values of 9.07 and –1.13 respectively, and their units agree with x and K in the Eq. (4). Therefore, as shown in Fig. 11, the corrosion reaction rate of the (Ag)–xxIn solid solution with sulfur vapor is exponentially decrease with the increase of indium concentration. In other words, the anti-tarnishing proper of (Ag)–xxIn solid solution is exponentially increasing with indium alloying concentration.

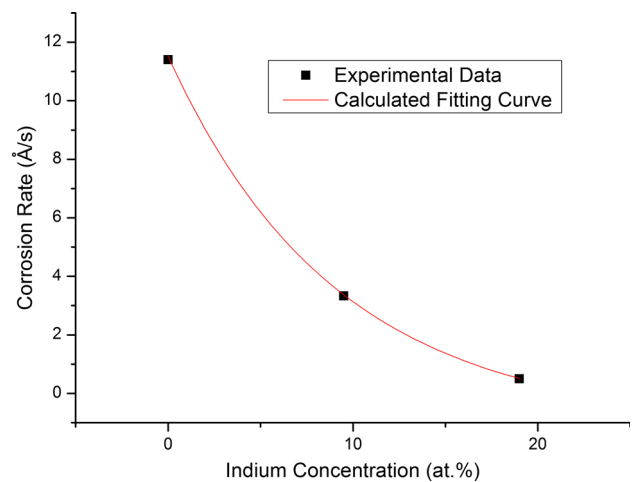


Fig. 11 The plot of silver sulfide growth rate versus indium concentration of (Ag)–xxIn solid solution

In conclusion, through this quantitative study of the sulfurization experiment, the sulfur gas corrosion reaction rate of pure silver, Argentium silver, (Ag)–9.5In and (Ag)–19In have been determined. The experimental results quantitatively confirm that the conclusion of previous observation under optical microscope. The correlation between the growth rate of silver sulfide and indium concentration have been made. Remarkably, (Ag)–19In exhibits fantastic anti-tarnishing property with repeatable experimental evidences.

5 Summary

In this paper, the grown methods for the materials of silver indium solid solution in ingots form have been described, following with the examine by SEM/EDX and XRD to confirm the composition and crystal structure of the materials. Furthermore, an accelerated quantitative corrosion test experiment has been designed to study the

tarnishing reaction between silver-based alloy and sulfur vapor. Previously, the anti-tarnishing property of silver-based alloy was used to be qualitatively described by the color or the reflectance of the tarnished surface of the sample. Details and insights of the design of experiment have been explained, and the results of testing experiment are accurate and repeatable. The qualitative observations under optical microscope are in agreement with quantitative measurement results, which can confirm the validity of the designed method. Therefore, this accelerated quantitative corrosion test experiment can potentially be used to develop standard test to evaluate anti-tarnishing property of silver-based alloy. In addition, the results of the sulfurization experiment of pure silver, Argentium, (Ag)–9.5In and (Ag)–19In have shown that (Ag)–xxIn solid solution exhibits excellent anti-tarnishing property, and the ability of anti-tarnishing exponentially increases with the indium element concentration. Significantly, the sulfurization reaction rate of (Ag)–19In is 22.8 times slower than of pure silver, 14.5 times slower than of Argentium silver. With the superior anti-tarnishing property, (Ag)–19In can be potentially used as the material in making jewelry, mirrors, and reflecting layers in LEDs devices.

Acknowledgments The authors would like to express our gratitude towards II-VI Foundation with Grant No. II-VI-104447, for its financial support during our academic research and to thank Dr. Shou-Jen Hsu for his assistance in setting up the hydrogen torch.

References

1. F.A. Cotton, G. Wilkinson, *Inorganic Chemistry*, 4th edn. (Wiley, New York, 1980)
2. C. Hillman, J. Arnold, S. Binfield, J. Seppi, Silver and sulfur: case studies, physics and possible solutions, in *Proceedings of SMTA International*, Orlando, FL. October, 2007
3. M.H. Hebb, Electrical conductivity of silver sulfide. *J. Chem. Phys.* **20**(1), 185–190 (1952)
4. D. Minzari, M.S. Jellesen, P. Moller, R. Ambat, Morphological study of silver corrosion in highly aggressive sulfur environments. *Eng. Fail. Anal.* **18**(8), 2126–2136 (2011)
5. G. Mura, G. Cassanelli, F. Fantini, M. Vanzi, Sulfur-contamination of high power white LED. *Microelectron. Reliab.* **48**(8), 1208–1211 (2008)
6. B.T. Reagor, J.D. Sinclair, Tarnishing of silver by sulfur vapor: film characteristics and humidity effects. *J. Electrochem. Soc.* **128**(3), 701–705 (1981)
7. H. Kim, Corrosion process of silver in environments containing 0.1 ppm H₂S and 1.2 ppm NO₂. *Mater. Corros.* **54**(4), 243–250 (2003)
8. X.Y. Mao, K.S. Tian, Tarnish mechanism of silver plating and anti-tarnish process. *Electroplat. Pollut. Control* **15**(1), 8–12 (1995)
9. J.D. Sinclair, Tarnishing of silver by organic sulfur vapors: rates and film characteristics. *J. Electrochem. Soc.* **129**(1), 33–40 (1982)
10. T.E. Graedel, Corrosion mechanisms for silver exposed to the atmosphere. *J. Electrochem. Soc.* **139**(7), 1963–1970 (1992)
11. C.J. Yang, C.H. Liang, X. Liu, Tarnishing of silver in environments with sulphur contamination. *Anti. Corros. Methods Mater.* **54**(1), 21–26 (2007)
12. R.R. Benham, Silver plating. *Anti. Corros. Methods Mater.* **10**(2), 31–35 (1963)
13. R. Bond, R.P. Stanek, W. Hoffman, Silver infrared reflective film, metal oxide dielectric film, silicon nitride protective coating; for windshields, windows, U.S. Patent, No. 5834103, issued Nov. 10, 1998
14. L. Paussaa, L. Guzman, E. Marina, N. Isomakib, L. Fedrizzia, Protection of silver surfaces against tarnishing by means of alumina/titania-nanolayers. *Surf. Coat. Technol.* **206**(5), 976–980 (2011)
15. C. Liang, C. Yang, N. Huang, Tarnish protection of silver by octadecanethiol self-assembled monolayers prepared in aqueous micellar solution. *Surf. Coat. Technol.* **203**(8), 1034–1044 (2009)
16. J. Randin, Chromated layer as an anti-tarnish protection of AuAgCu alloys. *Mater. Corros.* **43**(4), 172–176 (1992)
17. A. Butts, *Silver Economics Metallurgy and Use* (Huntington, R.E. Krieger Pub, 1967), pp. 123–136
18. J. Nielsen, J. Tuccillo, Tarnish resistant alloy, U.S. Patent, No. 3767391, issued Oct. 23, 1973
19. N. Sirirut, N. Ekasit, The anti-tarnishing, microstructure analysis and mechanical properties of sterling silver with silicon addition. *J. Met. Mater. Miner.* **12**(2), 13–18 (2003)
20. K.F. Edward, Silver alloy, U.S. Patent, No. 1970319, issued Aug. 14, 1934
21. P. Johns, Silver ternary alloy. U.S. Patent, No. 20070009375 A1, issued Jan. 11, 2007
22. D. Davitz, Alloy for jewelry with zinc, copper and silicon. U.S. Patent, No. 5882441, issued Mar. 16, 1999
23. Y. Huo, C.C. Lee, Anti-tarnishing evaluations of silver solid solution phase with indium, in *Electronic Components and Technology Conference (ECTC)*, 2015 IEEE 65th. IEEE, pp. 2180–2187, 2015
24. M.R. Baren, in *Binary Alloy Phase Diagrams*, ed. by T.B. Massalski, H. Okamoto (ASM Intl, Materials Park, 1990), pp. 47–48
25. A.N. Campbell, R. Wagemann, R.B. Ferguson, The silver–indium system: thermal analysis, photomicrography, electron microprobe, and X-ray powder diffraction results. *Can. J. Chem.* **48**(11), 1703–1715 (1970)
26. S. Lilienfeld, C.E. White, A study of the reaction between hydrogen sulfide and silver. *J. Am. Chem. Soc.* **52**(3), 885–892 (1930)
27. M. Beat, Elemental sulfur. *Chem. Rev.* **76**(3), 367–386 (1976)
28. D.W. Rice, P. Peterson, E.B. Rigby, P.B.P. Phipps, R.J. Cappell, R. Tremoureux, Atmospheric corrosion of copper and silver. *J. Electrochem. Soc.* **128**(2), 275–284 (1981)
29. P.R. Subramanian, J.H. Perepezko, The Ag–Cu (silver–copper) system. *J. Phase. Equilib.* **14**(1), 62–75 (1993)
30. A. Cusma, M. Sebastiani, D.D. Felicis, A. Basso, E. Bemporad, Study on the correlation between microstructure corrosion and wear resistance of Ag–Cu–Ge alloys. *Coatings* **5**(1), 78–94 (2015)